Eur. Phys. J. D **6**, 295–302 (1999)

THE EUROPEAN PHYSICAL JOURNAL D

EDP Sciences

Positronium formation cross-sections in the ground and excited states (n = 2 levels) in an e^+-He atom collision

B. Nath[a] and C. Sinha[b]

Department of Theoretical Physics, Indian Association for the Cultivation of Science, Jadavpur, Calcutta-700 032, India

Received: 20 July 1998 / Received in final form: 5 January 1999

Abstract. The positronium formation cross-sections in the ground and excited $n = 2$ levels have been studied in an e^+-He atom collision in the framework of eikonal approximation. Both the differential and total formation cross-sections have been investigated in the intermediate- and high-energy regime. Present eikonal results are found to differ appreciably from the corresponding first Born values even at very high incident energies. The total cross-section results have been compared with available experiments due to different groups as well as with other existing theoretical results.

PACS. 34.70.+e Charge transfer

1 Introduction

The study on the properties and production of positronium atom (Ps) leads one to an understanding of the validity of quantum electrodynamics [1]. Moreover such investigations provide us with fresh ideas about chemical reactions in which the active positive particle is of very small mass [2]. Another important stimulus to such investigations has come from the attempts made to understand the detected features of the spectrum of the electron positron annihilation radiation observed to be coming from the direction of the galactic centre and also from solar flares [3].

Due to the availability of more intense positron beams and sophisticated detectors, direct measurements of positronium (Ps) formation in positron-atom collisions have now become feasible. This, in turn, has stimulated the theoretical workers to study the Ps formation due to capture of an atomic electron by an incident positron beam from a neutral atomic target. Positronium formation cross-sections have recently been measured by a number of experimental workers [4–10] over a wide range of incident positron energies particularly for the neutral helium atom which is considered to be one of the most experimentally preferred targets. However, the experimental results of different groups do not agree satisfactorily over the entire energy range. As for the theoretical situation, a number of theoretical models have been proposed by different groups [11–24] for the calculation of Ps formation in a positron-helium atom collision for different ranges of incident e^+ energy. However the general agreement with the corresponding measurements is not very satisfactory, particularly in the intermediate- and high-energy domain. This gives added incentive to further theoretical investigation of the Ps formation from a helium atom specially for that energy region.

In the present work we study the differential as well as total Ps formation cross-sections for capture to ground and excited states ($2s$, $2p$) in a e^+-He collision at intermediate and high incident energies. The present calculations have been performed in the framework of eikonal approximation that takes account of higher-order effects which is essential for a rearrangement process especially at high incident energies where first Born approximation is not adequate.

Since the experimental results for Ps formation include the contributions from all energetically allowed states, theoretical cross-section data for capture to excited states are highly needed in order to make a meaningful comparison with the experiments. Expecting that the major contribution to excited state capture comes from the $n = 2$ level, the main emphasis is given on the calculation of Ps formation to the ground and excited $n = 2$ level only, in the present work. Further, assuming that the formation cross-section falls off as n^{-3}, the present calculation aslo allows the prediction of an estimate of the total Ps formation cross-sections at intermediate and high incident energies.

2 Theory

The expressions for the post and the prior form of the amplitude for Ps formation in the process $e^+ + He \longrightarrow (e^+e)(1s + 2s + 2p) + He^+(1s)$ are given as

$$T_{if}^{post} = \langle \Psi_f | V_f | \Psi_i^+ \rangle \,, \tag{1a}$$

$$T_{if}^{prior} = \langle \Psi_f^- | V_i | \Psi_i \rangle \,, \tag{1b}$$

[a] Kumar Ashutosh Institution (Main) Boys' 10/1, Dum Dum Road, Calcutta-700 030, India.

[b] e-mail: tpcs@mahendra.iacs.res.in

where $V_{\rm i}$ and $V_{\rm f}$ are the perturbations in the initial and final channels, respectively. In the present work we have chosen the post form (1a) since, for such rearrangement processes the post form of the amplitude might be more appropriate than the prior form [25,26].

In the framework of eikonal approximation the expression for $T_{\rm if}$ takes the form

$$T_{\rm if} = -\frac{\mu_f}{2\pi}\int \exp(-i\mathbf{k}_{\rm f}\cdot\mathbf{S})\exp(-\lambda_{\rm Ps}|\mathbf{r}_1-\mathbf{r}_2|) \times\left[\frac{Z}{r_1}-\frac{Z}{r_2}-\frac{1}{r_{13}}+\frac{1}{r_{23}}\right] \times\exp[(-\lambda_{\rm He^+})r_3]\Phi_{\rm He}(\mathbf{r}_2,\mathbf{r}_3)\exp(i\mathbf{k}_{\rm i}\cdot\mathbf{r}_1) \times(r_{12}-z_{12})^{-i\eta_{\rm i}}(r_1-z_1)^{i\eta_{\rm i}}\times{\rm d}\mathbf{r}_1{\rm d}\mathbf{r}_2{\rm d}\mathbf{r}_3\,, \quad (2)$$

where $\mathbf{r}_1$ and $\mathbf{r}_2$, $\mathbf{r}_3$ are, respectively, the position vectors of the incident positron (1) and the two bound electrons (2, 3) from the target nucleus which is taken to be infinitely heavy and at rest, $\mathbf{S}$ is the position vector of the centre of mass of the Ps atom with $\mathbf{S}=\frac{1}{2}|\mathbf{r}_1+\mathbf{r}_2|$ and $\eta_{\rm i}=\frac{1}{v}$, $\mathbf{v}$ being the velocity of the incident positron. $\mathbf{k}_{\rm i}$ and $\mathbf{k}_{\rm f}$ are the initial and final momenta and $\mu_{\rm f}$ is the three-body reduced mass in the final channel. In equation (2) $\lambda_{\rm Ps}(=1/2n)$ and $\lambda_{\rm He^+}(=2)$ are the bound-state parameters (in atomic units) for the Ps atom and He^+ ion, respectively. We have used atomic unit throughout our work. In constructing the initial channel wave function $\Psi_{\rm i}^+$ in equation (1) an assumption is made (for the sake of simplicity) that the incident positron is distorted only by the active electron (2) to be captured, while the role of the passive electron (3) is only to screen the positively charged nucleus by its negative charge cloud, thereby reducing the four-body problem to a three-body one in the final channel. This approximation should be legitimate for intermediate and high incident positron energies.

We now use the following contour integral [27] representations for the eikonal phase terms occurring in equation (2)

$$y^{\pm(i\eta-n)} = \frac{(-1)^{n+1}}{2i\sin(\mp\pi i\eta)\Gamma(\mp i\eta\pm n)} \times\int_c(-\lambda)^{\mp i\eta\pm n-1}\exp(-\lambda y){\rm d}\lambda\,, \quad (3)$$

where the contour c has branch cut from 0 to ∞. To obtain this, use has been made of the contour integral representation of the complex Γ function [27].

Thus, in view of equations (2) and (3), the expression for the amplitude $T_{\rm if}$ can now be written as (apart from some constants)

$$T_{\rm if} = \int_{c_1}\int_{c_2}\int\int\int \exp(-i\mathbf{k}_{\rm f}\cdot\mathbf{S})\exp(-\lambda_{\rm Ps}|\mathbf{r}_1-\mathbf{r}_2|) \times\left[\frac{Z}{r_1}-\frac{Z}{r_2}-\frac{1}{r_{13}}+\frac{1}{r_{23}}\right] \times\exp[(-\lambda_{\rm He^+})r_3]\Phi_{\rm He}(\mathbf{r}_2,\mathbf{r}_3)\exp(i\mathbf{k}_{\rm i}\cdot\mathbf{r}_1)p_1(\lambda_1,\mathbf{r}_1) \times p_2(\lambda_2,\mathbf{r}_{12})\times{\rm d}\mathbf{r}_1{\rm d}\mathbf{r}_2{\rm d}\mathbf{r}_3{\rm d}\lambda_1{\rm d}\lambda_2 \quad (4a)$$

where,

$$p_1(\lambda_1,\mathbf{r}_1)=\exp(-\lambda_1|r_1-z_1|)(-\lambda_1)^{-i\eta_{\rm i}-1}$$

and

$$p_2(\lambda_2,\mathbf{r}_{12})=\exp(-\lambda_2|r_{12}-z_{12}|)(-\lambda_2)^{i\eta_{\rm i}-1}, \quad (4b)$$

z_1 and z_{12} are the z components of the respective vectors $\mathbf{r}_1$ and $\mathbf{r}_{12}$, the z-axis being taken along the incident momentum direction $\mathbf{k}_{\rm i}$. The bound-state wave function of the He atom is chosen to be the uncorrelated Hylleraas type:

$$\Phi_{\rm He}(\mathbf{r}_2,\mathbf{r}_3)=N_{\rm i}\exp(-\lambda_{\rm i}r_2)\exp(-\lambda_{\rm i}r_3)\,, \quad (5)$$

where the screened parameter $\lambda_{\rm i}=1.6875$.

Substituting equation (4b) in (4a) we first perform the space integration over $\mathbf{r}_3$ analytically using standard Fourier transform technique so that all the four terms in equation (4a) become functions of $\mathbf{r}_1$ and $\mathbf{r}_2$ vectors only. The $\mathbf{r}_1$, $\mathbf{r}_2$ integrations are then carried out easily by using the same Fourier transform technique. The final result of the space integrations over $\mathbf{r}_1$, $\mathbf{r}_2$ and $\mathbf{r}_3$ in equation (4a) can be generated by suitable parametric differentiations from a basic integral of the type

$$I_0=\int_{c_1}\int_{c_2}{\rm d}\lambda_1{\rm d}\lambda_2(-\lambda_1)^{-i\eta-1}(-\lambda_2)^{i\eta-1} \times\int\frac{{\rm d}\mathbf{q}}{(q^2+\lambda^2)(|\mathbf{q}-\mathbf{q}_1|^2+\mu_1^2)(|\mathbf{q}-\mathbf{q}_2|^2+\mu_2^2)}. \quad (6)$$

The $\mathbf{q}$ integral in equation (6) has been performed analytically by Lewis [28] to obtain

$$J_0=\frac{\pi^2}{\sqrt{(\beta'^2-\alpha'\gamma')}}\ln\left[\frac{\beta'+\sqrt{(\beta'^2-\alpha'\gamma')}}{\beta'-\sqrt{(\beta'^2-\alpha'\gamma')}}\right], \quad (7)$$

with

$$\beta'=\lambda[|\mathbf{q}_1-\mathbf{q}_2|^2+(\mu_1+\mu_2)^2]+\mu_2(\lambda^2+q_1^2+\mu_1^2) +\mu_1(\lambda^2+q_2^2+\mu_2^2)$$

and

$$\alpha'\gamma'=[(\mathbf{q}_1-\mathbf{q}_2)^2+(\mu_1+\mu_2)^2][q_1^2+(\mu_1+\lambda)^2] \times[q_2^2+(\mu_2+\lambda)^2], \quad (8)$$

where α', β' and γ' are functions of the momenta ($\mathbf{k}_{\rm i}$, $\mathbf{k}_{\rm f}$) and bound-state parameters ($\lambda_{\rm Ps}$, $\lambda_{\rm He^+}$, $\lambda_{\rm i}$) as well as of the integration variables λ_1 and λ_2.

Instead of using this analytic form of J_0 which contains a logarithmic branch cut we use the following contour-integral representation as first suggested by Sinha and Sil [29],

$$J_0=2\pi^2\int_0^\infty\frac{{\rm d}x}{\alpha'x^2+2\beta'x+\gamma'}\,, \quad (9)$$

where the product $\alpha'\gamma'$ has been split in such a manner that both α' and γ' are individual linear functions of the

integration variables λ_1 and λ_2. By virtue of this choice we can perform λ_1 and λ_2 integrations analytically. In view of equation (6) and equation (9) we arrive at the following type of integral:

$$I_0 = \int_0^\infty \int_{c_1} \int_{c_2} \frac{(-\lambda_1)^{-i\eta_i - 1}(-\lambda_2)^{i\eta_i - 1}}{(A + B\lambda_1 + C\lambda_2 + D\lambda_1\lambda_2)} \mathrm{d}x\, \mathrm{d}\lambda_1 \mathrm{d}\lambda_2, \quad (10)$$

where the contour c_1, c_2 refer to the same as that in equation (3a). In equation (10), A, B, C and D are functions of the $\mathbf{k}_i$, $\mathbf{k}_f$, λ_i, λ_f, λ_{Ps} and the integration variable x. Now in order to perform the λ_1 and λ_2 integrations analytically, we recast equation (10) in the following manner:

$$I_0 = \int_0^\infty \frac{1}{A} \int_{c_1} \int_{c_2} \frac{p_1(\lambda_1) p_2(\lambda_2)}{(1+\alpha\lambda_1)(1+\beta\lambda_2)(1+z)} \mathrm{d}x\, \mathrm{d}\lambda_1 \mathrm{d}\lambda_2, \quad (11a)$$

where

$$\alpha = B/A,\ \beta = C/A,\ \gamma = D/A,\ z = \frac{(\gamma - \alpha\beta)\lambda_1\lambda_2}{(1+\alpha\lambda_1)(1+\beta\lambda_2)}$$

and

$$p_1(\lambda_1) = (-\lambda_1)^{-i\eta_i - 1}, p_2(\lambda_2) = (-\lambda_2)^{i\eta_i - 1}. \quad (11b)$$

For the evaluation of the integral (11a) we first assume that z is a very small quantity, although this restriction will be relaxed afterwards. Using the binomial expression of $(1+z)^{-1}$ in equation (11a), we obtain

$$I_0 = \int_0^\infty \frac{1}{A} \sum_{n=0}^{\infty} \int_{c_1} \int_{c_2} p_1(\lambda_1) p_2(\lambda_2) \times \frac{(-1)^n (\gamma - \alpha\beta)^n \lambda_1^n \lambda_2^n}{(1+\alpha\lambda_1)^{n+1}(1+\beta\lambda_2)^{n+1}} \mathrm{d}\lambda_1 \mathrm{d}\lambda_2 \mathrm{d}x. \quad (12)$$

Now if the integrated expression of I_0 becomes an analytic function of z (which happens to the case here, as may be noted below) the above binomial expression in equation (12) will be valid for all values of z by virtue of analytic continuation.

The λ_1 and λ_2 integrations in equation (12) are now separable and each term of the series can be integrated by the residue calculation method. The nth-order term of the series contains a pole of $(n+1)$th order and thus involves a nth-order differentiation in the residue calculation method. To show how the λ_1 or λ_2 integration is performed analytically, let us first consider the following basic integral:

$$I = \int_c \frac{p_1(\lambda_1)}{(1+\alpha\lambda_1)} \mathrm{d}\lambda_1 = \int_c f(\lambda_1) \mathrm{d}\lambda_1 \text{ (say)}. \quad (13)$$

Now in equation (13) it is noted that the modulus of the function f is of the order of $1/|\lambda_1|^2$ as $|\lambda_1| \to \infty$, *i.e.*

$$|f(\lambda_1)| \propto 1/|\lambda_1|^2 \text{ as } |\lambda_1| \to \infty. \quad (14)$$

Further, the function f contains a simple pole lying outside the contour c. Thus by Cauchy's residue theorem we have

$$\int_c \frac{p_1(\lambda_1)}{(1+\alpha\lambda_1)} \mathrm{d}\lambda_1 + 2\pi i \text{ (residue at the pole } \lambda_1^* = -1/\alpha) = \int_{c_\infty : |\lambda_1| = R, R \to \infty} \frac{p_1(\lambda_1)}{\lambda_1 - \lambda_1^*} \mathrm{d}\lambda_1. \quad (15)$$

Now since the right-hand side of (15) vanishes, we find from equation (13),

$$I = \frac{1}{\alpha} \int_c \frac{p_1(\lambda_1)}{\lambda_1 - \lambda_1^*} \mathrm{d}\lambda_1 = -2\pi i \text{ (residue at } \lambda_1^*) = -2\pi i (\alpha)^{i\eta_i}. \quad (16)$$

Similarly the λ_2 integration is then carried out following the same technique since the corresponding function f for λ_2 satisfies the same condition as in equation (14). The final result of λ_1, λ_2 integrations in equation (12), the integrand of which contains $(n+1)$th-order poles in λ_1 and λ_2, is obtained by performing nth-order differentiations of the integrated results of the basic λ_1 and λ_2 integrals (*e.g.* I in equation (16), for λ_1) with respect to α and β, respectively. The final expressions for λ_1 and λ_2 integrations in equation (12) are given by

$$\int_{c_1} \frac{\lambda_1^n (-\lambda_1)^{-i\eta_i - 1}}{(1+\alpha\lambda_1)^{n+1}} \mathrm{d}\lambda_1 = \int_{c_1} I_{\lambda_1} \mathrm{d}\lambda_1 = \frac{2\pi i}{n!} (-i\eta_i)_n \alpha^{i\eta_i - n},$$

and

$$\int_{c_2} \frac{\lambda_2^n (-\lambda_2)^{i\eta_i - 1}}{(1+\beta\lambda_2)^{n+1}} \mathrm{d}\lambda_2 = \int_{c_2} I_{\lambda_2} \mathrm{d}\lambda_2 = \frac{2\pi i}{n!} (i\eta_i)_n \beta^{-i\eta_i - n}. \quad (17)$$

Thus in view of equations (12, 17) and (11b) we arrive at the following expression:

$$I_0 = -4\pi^2 \int_0^\infty \frac{1}{A} \left[\frac{B}{A}\right]^{i\eta_i} \left[\frac{C}{A}\right]^{-i\eta_i} {}_2F_1(-i\eta_i, i\eta_i, 1, z') \mathrm{d}x, \quad (18)$$

where $z' = 1 - \frac{AD}{BC}$ and ${}_2F_1$ denotes the hypergeometric function with argument z'. We are thus finally left with the x integral which has been evaluated numerically by using Gaussian quadrature method. The actual integrals occurring from the expression of T_{if} in equation (2) are then derived from I_0 by parametric differentiations.

3 Results and discussions

The Ps formation cross-section results, both differential and total have been computed for the process $e^+ + He(1s) \longrightarrow (e^+e)(1s, 2s, 2p) + He^+(1s)$ in the framework of eikonal approximation.

Figures 1-3 exhibit the present differential cross-sections in the ground and excited $(2s, 2p)$ states at incident positron energies 75 eV, 100 eV and 500 eV, respectively. The differential cross-section at energy 75 eV (Fig. 1) shows a sharp minimum at the angle $\sim 30^\circ$ for the

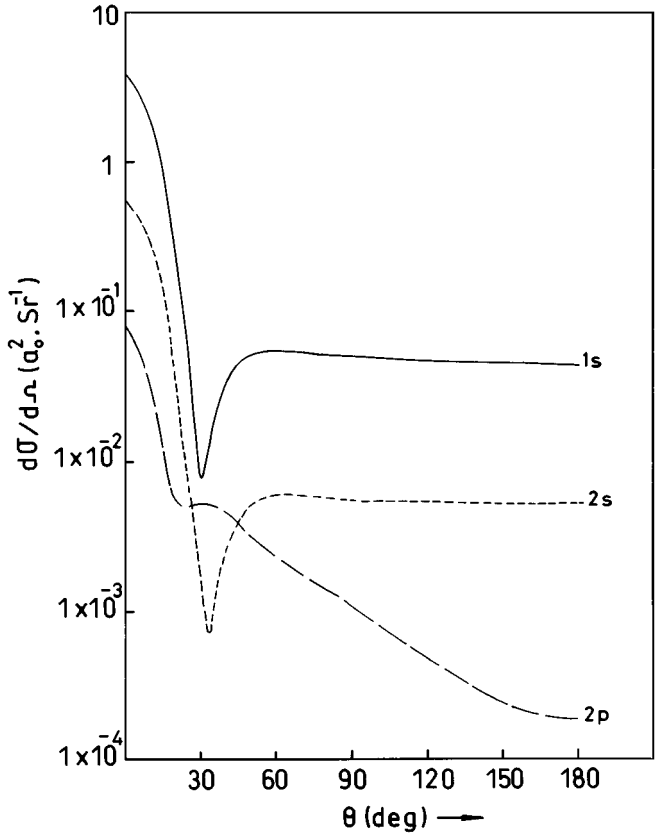

Fig. 1. Differential cross-sections ($1s$, $2s$, $2p$) (in $a_0^2 \cdot \mathrm{Sr}^{-1}$) for positronium formation in positron-helium atom collisions for incident energy $E = 75$ eV, solid line for $1s$, dashed line for $2s$ and long-dashed line for $2p$ states.

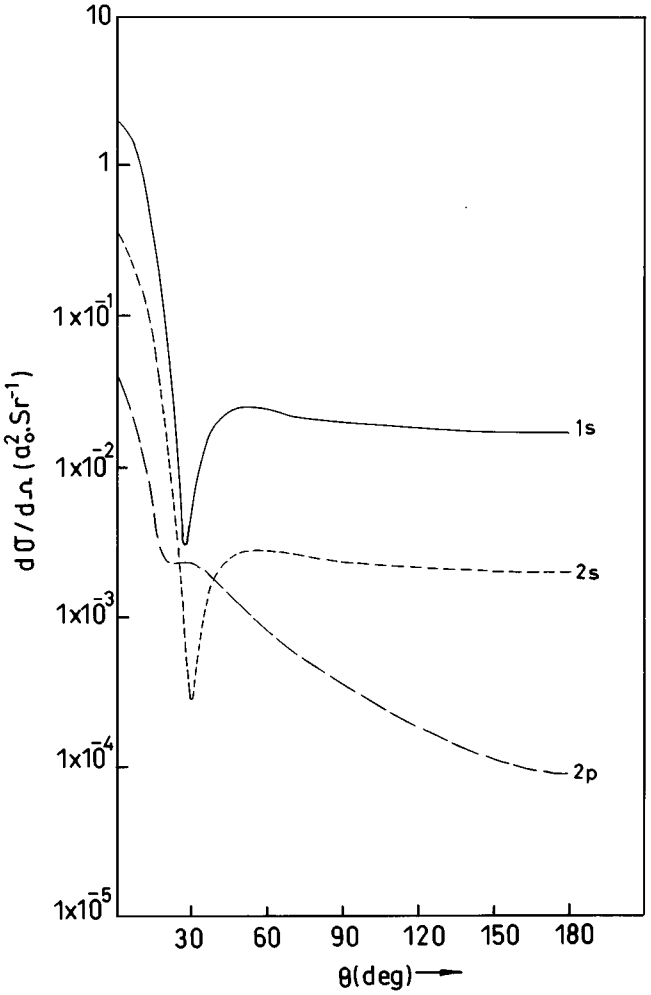

Fig. 2. Same as Figure 1 but with incident energy $E = 100$ eV.

$1s$ and $2s$ states, while for the $2p$ states the curve falls almost monotonically as the angle increases except for a dip occurring at an angle $< 30°$. With increasing energy the minima for the $1s$, $2s$ as well as the kink for the $2p$ curves shift towards smaller angles (see Figs. 2 and 3). Further, a secondary minima starts appearing with increasing incident energy (*e.g.*, 500 eV, 10000 eV, in Figs. 3 and 4) and gets more and more pronounced with increasing energy (see Fig. 4 for 10000 eV). Figure 4 shows the prominent occurrence of these two minima for both $1s$ and $2s$ states.

The occurence of the first minimum in the $1s$ and $2s$ differential curves may be ascribed to the fact that the contributions from the attractive and the repulsive parts of the interaction potential to the scattering amplitude interfere destructively at this angle. Since with increasing energy both the amplitudes for attractive and repulsive parts become more and more peaked in the forward direction, the position of the minimum (due to the destructive interference between the two) shifts towards smaller angles as the energy increases. The minima for the m-degenerate states occur at different scattering angles and, as a result, the total differential cross-sections for the $2p$ state do not exhibit such a minimum [30]. The appearance of the secondary minima at higher incident energies (*e.g.*, Fig. 4) for the $1s$ and $2s$ differential and the single minimum for the $2p$ differential curves may be attributed to the second-order effect. It should be pointed out here that no such secondary minimum occurs in the FBA results even at very high energy (*e.g.*, 10000 eV). We have also computed the present differential cross-sections at some extreme high energy (~ 50 keV) (not shown in the figure) and have noted that no other minimum appears in the differential curves.

Figure 5 displays the partial total cross-sections (TCS) for capture into $1s$, $2s$ and $2p$ states for the incident energy range 50-250 eV. Since the present approximation is basically a high-energy one, results below 50 eV are not expected to be very meaningful. As noted from Figure 5, the magnitude of the TCS is in decreasing order for $1s$, $2s$ and $2p$ states for a particular incident energy and the TCS curve for all the states falls monotonically with increasing energy, as expected.

Figure 6 compares the present TCS with some available experimental data [4,5,8,9] due to different groups as well as with some other theoretical results [11–16]. Although Figure 6 displays the total Ps formation cross-sections throughout the energy range (0-250 eV), comparison of the present results with experiments and theories

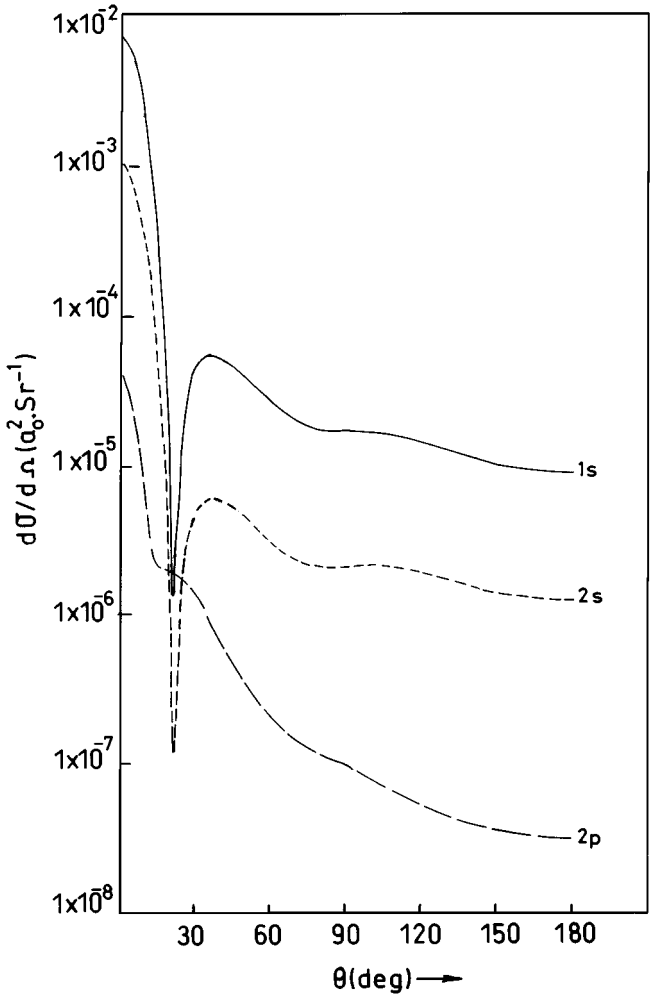

Fig. 3. Same as Figure 1 but with incident energy $E = 500$ eV.

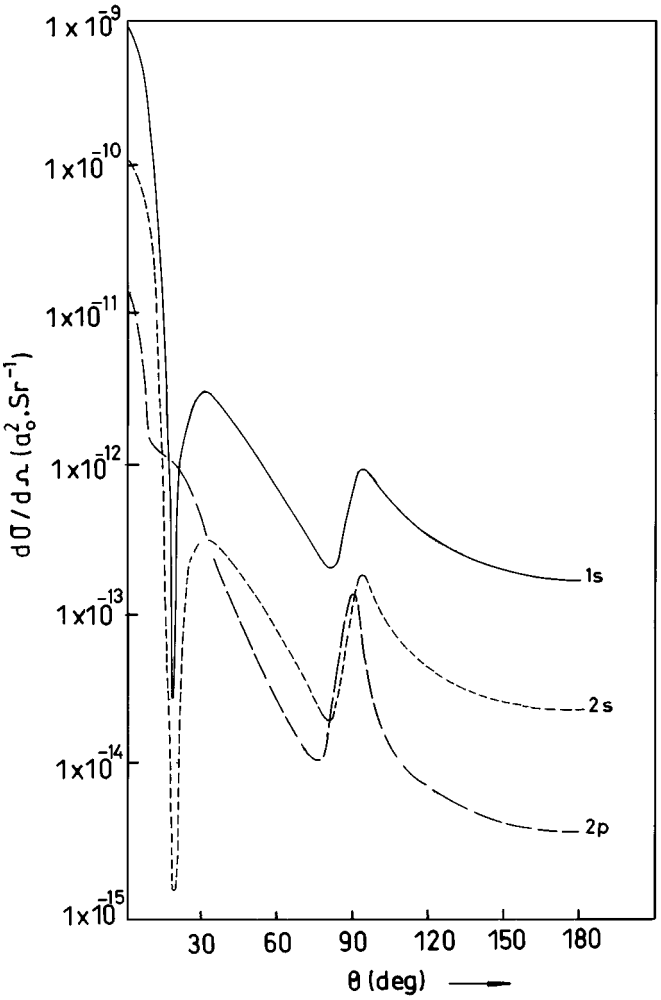

Fig. 4. Same as Figure 1 but with incident energy $E = 10000$ eV, and $2p$ results are multiplied by a factor of 100.

will be made only in the intermediate- and high-energy region since the present model is based on high-energy approximation.

It is evident from Figure 6 (as also mentioned in the Introduction) that the experimental data obtained by the different groups do not agree with each other throughout the energy region. However, as may be noted from Figure 6, the present TCS result agrees most with one of the most current experimental data of Overton *et al.* [5]. The present TCS curve lies always below the measurements [5] except at low energies where the present model is not supposed to be very reliable. At intermediate- and high-energy region the underestimation of the present results as compared to the experiment [5] appears to be legitimate since the measurement includes the contributions for capture to all possible excited states whereas the present results represent only the $\sigma = 1s + 2s + 2p$ results.

As for the comparison with some other theoretical results in Figure 6, it may be noted that the present $\sigma_{\rm Ps}(1s + 2s + 2p)$ are in reasonably good agreement with the close coupling results of Hewitt *et al.* [11] at and above 100 eV. Below 100 eV (80-30 eV) the present $1s$ results overestimate, while the $2p$ results underestimate the results of Hewitt *et al.* (see Table 2 in Ref. [11]). In contrast, for the $2s$ state, the two results agree well throughout the energy range. However, the agreement of the present results with the close coupling (cc) results of Chaudhuri and Adhikari [13] is not so good except at very high energies (200 eV and above). The summed Ps formation result $\sigma_{\rm Ps}(1s + 2s + 2p)$ of Chaudhuri and Adhikari [13] lies always above the corresponding present result above 100 eV, till it converges to the latter at about 250 eV. It may also be noted from Figure 6 that the present results also agree well with the coupled static approximation (CSA) results of McAlinden and Walters [12], particularly in the high-energy region (above 100 eV), although the latter always lies below the former one. This might be due to the fact that the CSA results [12] correspond to Ps formation in the gronud ($1s$) state only while the present results correspond to $(1s + 2s + 2p)$ state.

Regarding the agreement of the other theoretical results with the measurements, it may be noted from Figure 6 that almost all the theoretical results (except [15, 16]) are more or less in reasonable agreement with the most current experimental data [5] in the high-energy

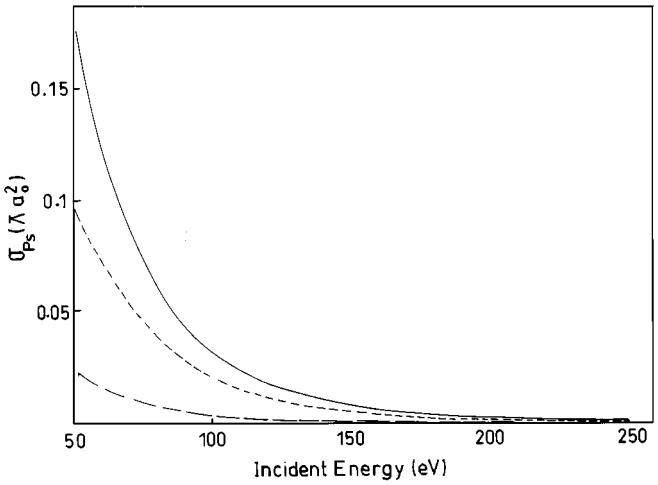

Fig. 5. Partial total cross-sections (in πa_0^2) for positronium formation in positron-helium atom collision of $1s$, $2s$ and $2p$ for the energy range from 50 eV to 250 eV, solide line for $1s$, dashed line for $2s$ and long-dashed line for $2p$. Here $1s$ results divided by a factor of 5.

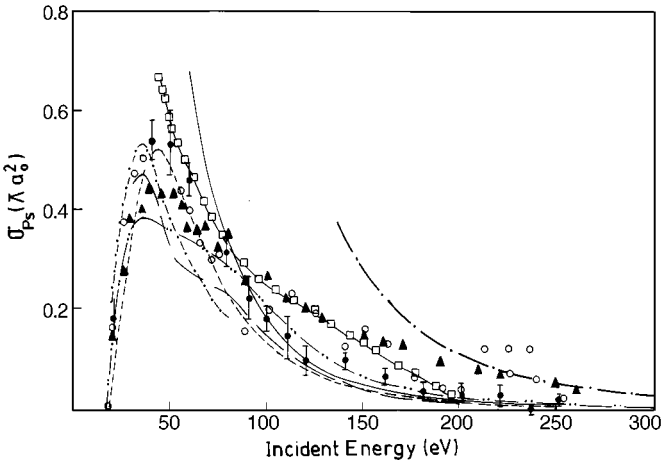

Fig. 6. Total cross-sections (in 10^{-16} cm ^{2}) for positronium formation in positron-helium atom collisions. Solid line: present calculation; close circles: experimental results of Overton *et al.* (1993); close triangles: measurement of Fromme *et al.* (1986); open circles: Fornari *et al.* (1983) and Diana *et al.* (1986); dashed line: coupled static approximation, McAlinden and Walters (1992); long-dashed line: close coupling approximation, Hewitt *et al.* (1991); long-dashed-dot line: Deb *et al.* (1990); dashed-dot line: Khan *et al.* (1985); open squares: calculation of McDowell and Peach as reported by Formme *et al.* (1986); double-dotted-dashed line: Chaudhuri *et al.* (1998).

regime ($\sim$ 100 eV onwards). Further, Figure 6 also reveals that the theoretical cross-sections do not show any oscillatory structure in the high-energy region as in the measurements of Diana *et al.* [8]. Thus the theoretical results corroborate the findings of the other two measurements [4,5] in this respect. In the high-energy regime, the measurements of Fromme *et al.* [4] and Diana *et al.* [8] are well above the theories (except the two results [15, 16] based on high-energy approximations). However, in the low-energy region the theoretical results of McAlinden and Walters [12] and the distorted wave approximation (DWA) results of Khan *et al.* [14] are in close agreement with the measurements of Diana *et al.*, Fornari *et al.* [8,9] although the positions of the low-energy peak are slightly shifted. It may further be noted from Figure 6 that in both the close coupling results [11,13], particularly the latter one, the magnitude of the low-energy peak is well below the experiments [5,8,9]. Figure 6 also includes two other theoretical results based on high-energy approximations. The TCDW1 results of Deb *et al.* [16] are quite far from the present results throughout the energy range considered. In fact the TCDW1 results agree only with the measurement of Fromme *et al.* [4] and that is also only at high incident energies (*i.e.* from 200 to 300 eV). Regarding the other theoretical results [15] displayed in Figure 6, the present TCS curve crosses that due to McDowell and Peach [15] only at a particular incident energy while below and above the crossing their results are always higher than the present ones. The discrepancy increases with increasing incident energy. However, the results of McDowell and Peach agree well with the measurements of Fromme *et al.* [4] at intermediate energies ($<$ 200 eV), while they are quite apart from the measurements of Overton *et al.* [5] in the energy range $\sim$ 90-160 eV.

Table 1 displays the present partial cross-section values for the $1s$, $2s$ and $2p$ states for various incident energies along with the corresponding Born results.

It is evident from Table 1 that, at energies below 80 eV, the present $1s$ and $2s$ results always overestimate the First Born Approximation. But above 80 eV, the eikonal results approach the corresponding FBA results, coincide at a particular energy depending on the state to which the capture is taking place, and then continue to lie much below the Born approximation results throughout the energy region. In contrast, for the $2p$ state, the energy is 50 eV below which the present results overestimate the FBA values. Further, for the $2p$ state the discrepancy between the FBA and the eikonal results is much higher than for the $1s$ and $2s$ states for energies above 80 eV. In fact, the percentage of discrepancy (for the case of $2p$ state) increases with increasing incident energy.

It is also apparent from Table 1 that the present ($n=2$) level capture cross-sections ($\sigma_{2s} + \sigma_{2p}$) are always higher than the corresponding FBA values below 80 eV, while from 80 eV onwards, they always lie below the FBA values. This feature is also maintained in the behaviour of the total ($\sigma_{1s} + \sigma_{2s} + \sigma_{2p}$) Ps formation cross-sections in the present approximation, but at a different energy (*e.g.*, $>$ 90 eV).

It may further be inferred from Table 1 that the present Ps formation cross-sections ($1s$, $2s$, $2p$) do not converge to the corresponding FBA results even at an energy as high as 10000 eV. This may be attributed to the fact that for very high incident energies, the FBA model is not adequate for a rearrangement collision process; the

Table 1. Ps formation cross-sections for the process $e^+ + He(1s) \rightarrow (e^+e)(1s + 2s + 2p) + He^+$ (in units of πa_0^2). The numbers in square brackets indicate the power of 10 by which the entry is to be multiplied (pr: present work).

eV	FAB	pr $(1s-1s)$	FAB	pr $(1s-2s)$	FAB	pr $(1s-2p)$	pr $(1s+2s+2p)$
30	1.54	1.69	1.16 [−1]	1.04 [−1]	2.92 [−2]	4.20 [−2]	1.84
40	1.18	1.31	1.15 [−1]	1.20 [−1]	2.66 [−2]	3.18 [−2]	1.46
50	8.40 [−1]	9.10 [−1]	9.24 [−1]	9.71 [−2]	2.11 [−2]	2.26 [−2]	1.03 [−1]
60	5.86 [−1]	6.30 [−1]	6.69 [−2]	7.25 [−2]	1.56 [−2]	1.55 [−2]	7.18 [−1]
70	4.14 [−1]	4.30 [−1]	5.14 [−2]	5.28 [−2]	1.12 [−2]	1.06 [−2]	4.93 [−1]
80	2.97 [−1]	3.04 [−1]	3.79 [−2]	3.83 [−2]	7.97 [−3]	7.23 [−3]	3.49 [−1]
100	1.60 [−1]	1.60 [−1]	2.10 [−2]	2.06 [−2]	4.09 [−3]	3.49 [−3]	1.84 [−1]
125	8.03 [−2]	7.64 [−2]	1.07 [−2]	1.02 [−2]	1.87 [−3]	1.52 [−3]	8.81 [−2]
150	4.35 [−2]	4.10 [−2]	5.85 [−3]	5.38 [−3]	9.22 [−4]	7.18 [−4]	4.62 [−2]
175	2.50 [−2]	2.25 [−2]	3.38 [−3]	3.03 [−3]	4.83 [−4]	3.64 [−4]	2.59 [−2]
200	1.52 [−2]	1.33 [−2]	2.05 [−3]	1.79 [−3]	2.68 [−4]	1.97 [−4]	1.53 [−2]
300	2.95 [−3]	2.42 [−3]	3.95 [−4]	3.24 [−4]	3.82 [−5]	2.60 [−5]	2.77 [−3]
400	8.40 [−4]	6.60 [−4]	1.11 [−4]	8.77 [−5]	8.49 [−6]	5.52 [−6]	7.53 [−4]
500	3.02 [−4]	2.30 [−4]	3.98 [−5]	3.04 [−5]	2.49 [−6]	1.57 [−6]	2.62 [−4]
700	6.05 [−5]	4.41 [−5]	7.89 [−6]	5.77 [−6]	3.62 [−7]	2.17 [−7]	5.01 [−5]
1000	1.02 [−5]	7.10 [−6]	1.32 [−6]	9.22 [−7]	4.26 [−8]	2.44 [−8]	8.05 [−6]
2000	2.65 [−7]	1.72 [−7]	3.37 [−8]	2.21 [−8]	5.30 [−10]	2.85 [−10]	1.94 [−7]
3000	2.86 [−8]	1.80 [−8]	3.62 [−9]	2.30 [−9]	3.67 [−11]	1.93 [−11]	2.03 [−8]
4000	5.70 [−9]	3.50 [−9]	7.19 [−10]	4.50 [−10]	5.34 [−12]	2.79 [−12]	3.95 [−9]
8000	1.08 [−10]	6.51 [−11]	1.36 [−11]	8.30 [−12]	4.79 [−14]	2.49 [−14]	7.34 [−11]
10000	2.96 [−11]	1.77 [−11]	3.27 [−12]	2.26 [−12]	1.03 [−14]	5.42 [−15]	1.10 [−11]

higher-order effects (incorporated in the present model) should also be taken into account.

Table 1 also indicates that the cross-section $\sigma_{2p} < \sigma_{2s} < \sigma_{1s}$ and at very high incident energies the ratio of $\sigma_2 (= \sigma_{2s} + \sigma_{2p})$ and σ_1 (*i.e.* σ_{1s}) approaches the value 0.128 (*e.g.*, at 10000 eV), approximately satisfying the n^{-3} rule (n being the principal quantum number). It may be mentioned here that for the case of hydrogen atom as target, the n^{-3} law is exactly satisfied at high incident energy whereas for helium atom the ratio approaches almost asymptotically the n^{-3} value for high incident energies. For example, even at an incident energy as high as 20000 eV, the above ratio is found to be 0.128. In view of this n^{-3} law it is thus expected that the contributions from the higher states ($n > 2$) will decrease gradually and hence it would be quite reasonable to predict from the cross-sections σ_1 and σ_2, an estimate for the total Ps formation cross-section.

Finally it may be inferred (from Fig. 6) that in most of the theoretical results (except [15,16]) the behaviour of the σ_{Ps} (*i.e.* fall of σ_{Ps}) with respect to the incident positron energy at intermediate energies is more or less in conformity with the findings of Overton *et al.* [5] ($\sim E^{-2.5}$) while the earlier measurements [4,8,9] show a much slower fall off ($\sim E^{-1}$).

References

1. M.A. Stroscio, Phys. Rep. C **22**, 215 (1975).
2. P.A. Fraser, Adv. At. Mol. Phys. **4**, 63 (1968).
3. J.W. Humberston, Adv. At. Mol. Phys. **22**, 1 (1986).
4. D. Fromme, G. Kruse, W. Raith, G. Sinapius, Phys. Rev. Lett. **57**, 3031 (1986).
5. N. Overton, R.J. Mills, P.G. Coleman, J. Phys. B: At. Mol. Opt. Phys. **26**, 3951 (1993).
6. J. Moxom, G. Laricchia, M. Charlton, J. Phys. B: At. Mol. Opt. Phys. **26**, L367 (1993).
7. J. Moxom, G. Laricchia, M. Charlton, A. Kovar, W.E. Meyerhof, Phys. Rev. A **50**, 3129 (1994).
8. L.M. Diana, P.G. Coleman, D.L. Brooks, P.K. Pendleton, D.M. Norman, Phys. Rev. A **34**, 2731 (1986).
9. L.S. Fornari, L.M. Diana, P.G. Coleman, Phys. Rev. Lett. **51**, 2276 (1983).
10. M. Charlton, G. Laricchia, J. Phys. B: At. Mol. Opt. Phys. **23**, 1045 (1990).
11. R.N. Hewitt, C.J. Noble, B. H. Bransden, J. Phys. B: At. Mol. Opt. Phys. **25**, 557 (1992).
12. M.T. McAlinden, H.R.J. Walters, Hyperfine Int. **73**, 65 (1992).
13. P. Chaudhuri, S.K. Adhikari, J. Phys. B: At. Mol. Opt. Phys. **31**, 3057 (1998).
14. P. Khan, P.S. Mazumdar, A.S. Ghosh, Phys. Rev. A **31**, 1405 (1985).
15. M.R.C. McDowell, G. Peach, 1985 private communication (as referenced by Fromme *et al.* (1986)).

16. N.C. Deb, D.S.F. Crothers, D. Fromme, J. Phys. B: At. Mol. Opt. Phys. **23**, L483 (1990).
17. P. Mondal, S. Guha, N.C. Sil, J. Phys. B: At. Mol. Opt. Phys. **12**, 2913 (1979).
18. P. Khan, A.S. Ghosh, Phys. Rev. A **28**, 2181 (1983).
19. N.C. Deb, J.H. McGuire, N.C. Sil, Phys. Rev. A **36**, 3707 (1987); *ibidem*, Phys. Rev. A **36**, 1082 (1987).
20. M.J. Roberts, J. Phys. B: At. Mol. Opt. Phys. **22**, 3315 (1989).
21. D.R. Schultz, R.E. Olson, Phys. Rev. A **38**, 1866 (1988).
22. A. Igarashi, I. Toshima, Phys. Lett. A **164**, 70 (1992).
23. N.K. Sarkar, M. Basu, A.S. Ghosh, Phys. Rev. A **45**, 6887 (1992).
24. P. Chaudhuri, S.K. Adhikari, A.S. Ghosh, J. Phys. B: At. Mol. Opt. Phys. **30**, L81 (1997).
25. D.S.F. Crothers, Proc. Phys. Soc. **91**, 855 (1967).
26. C. Sinha, S. Tripathi, N.C. Sil, Phys. Rev. A **34**, 1026 (1986).
27. I.S. Gradshteyn, I.M. Ryzhik, *Tables and Integrals, Series and Products* (Academic, New York, 1980) p. 933.
28. R.R. Lewis jr., Phys. Rev. **102**, 537 (1956).
29. C. Sinha, N.C. Sil, J. Phys. B **11**, L333 (1978).
30. N.C. Sil, B.C. Saha, H.P. Saha, P. Mondal, Phys. Rev. A **19**, 655 (1979).